Integrative Biology

Cite this: *Integr. Biol.*, 2011, **3**, 1033–1042

www.rsc.org/ibiology

PAPER

Mechanotransductional basis of endothelial cell response to intravascular bubbles†

Alexandra L. Klinger, Benjamin Pichette, Peter Sobolewski and David M. Eckmann*

Received 17th February 2011, Accepted 23rd August 2011
DOI: 10.1039/c1ib00017a

Vascular air embolism resulting from too rapid decompression is a well-known risk in deep-sea diving, aviation and space travel. It is also a common complication during surgery or other medical procedures when air or other endogenously administered gas is entrained in the circulation. Preventive and post-event treatment options are extremely limited for this dangerous condition, and none of them address the poorly understood pathophysiology of endothelial response to intravascular bubble presence. Using a novel apparatus allowing precise manipulation of microbubbles in real time fluorescence microscopy studies, we directly measure human umbilical vein endothelial cell responses to bubble contact. Strong intracellular calcium transients requiring extracellular calcium are observed upon cell-bubble interaction. The transient is eliminated both by the presence of the stretch activated channel inhibitor, gadolinium, and the transient receptor potential vanilliod family inhibitor, ruthenium red. No bubble induced calcium upsurge occurs if the cells are pretreated with an inhibitor of actin polymerization, cytochalasin-D. This study explores the biomechanical mechanisms at play in bubble interfacial interactions with endothelial surface layer (ESL) macromolecules, reassessing cell response after selective digestion of glycocalyx glycosoaminoglycans, hyaluran (HA) and heparin sulfate (HS). HA digestion causes reduction of cell-bubble adherence and a more rapid induction of calcium influx after contact. HS depletion significantly decreases calcium transient amplitudes, as does pharmacologically induced sydencan ectodomain shedding. The surfactant perfluorocarbon Oxycyte abolishes any bubble induced calcium transient, presumably through direct competition with ESL macromolecules for interfacial occupancy, thus attenuating the interactions that trigger potentially deleterious biochemical pathways.

Introduction

Gas embolism, the abnormal presence of gas bubbles in the vasculature, is classically associated with decompression sickness, a well-known risk in deep sea diving, aviation or space travel. Gas embolism is more common, however, as a complication in surgical or non-operative medical procedures

Department of Anesthesiology and Critical Care, University of Pennsylvania, Philadelphia, PA 19104, USA. E-mail: eckmanndm@uphs.upenn.edu; Fax: 215 349 5078; Tel: 215 349 5348

† Electronic supplementary information (ESI) available. See DOI: 10.1039/c1ib00017a

Insight, innovation, integration

Specific molecular mechanisms by which cells sense mechanical forces and translate them to intracellular signaling responses remain poorly understood. Endothelial mechotransductional responses to contact with gas/liquid interfaces in bubble embolism are not well characterized, and clinical options for the treatment of gas embolism related injury are extremely limited. Herein, through integration of live-cell imaging with a novel apparatus allowing precise manipulation of microbubbles, we directly measure endothelial cell response to bubble contact. These studies reveal specific gas/liquid interfacial interactions with endothelial surface layer components that initiate spurious bubble-induced intracellular Ca^{2+} transients and demonstrate surfactant intervention of the triggering interactions for Ca^{2+} response. This work provides insight into apical mechanical signal transduction architecture by specific application of force to this surface.

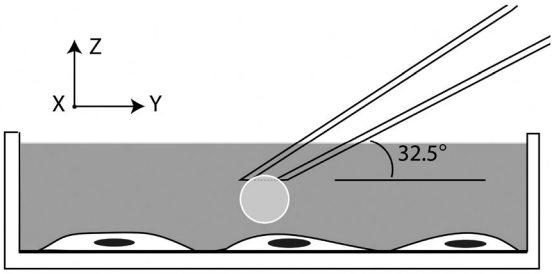

Fig. 1 Schematic of bubble probing apparatus (described in Methods) to bring bubble, on the end of a pulled and ground glass capillary tip, in contact with cells for time-lapse fluorescent microscopy imaging studies.

if air or other exogenously delivered gas is entrained in the circulation. Clinical manifestations vary widely, but may be catastrophic, especially if the bubble becomes lodged in the cerebral, pulmonary or cardiac circulation. Lesser non-ischemic manifestations, associated with cerebrovascular gas embolism, are reduced consciousness, seizure and cognitive impairment. These effects have been well characterized as neurological complications in cardiac surgery, but preventative and post-event treatment options for central nervous system gas embolism remain extremely limited. In fact, root causes of vascular air embolic injury—endothelial molecular signaling responses to the bubble and the mechanisms by which these responses are triggered by surface interfacial interactions—are poorly understood.

The gas/liquid interface presented by a bubble is a physio-chemically active surface to which blood and endothelial surface layer (ESL) proteins have been shown to partition and subsequently unfold.[1–3] Our working hypothesis is that surface interactions between the bubble and macromolecules of the endothelium within the compromised vessel initiate pathophysiological events leading to endothelial cell injury and aberrant behavior. We further posit that a surfactant based therapeutic strategy would be effective in reducing triggering interactions by populating the gas/liquid interface with preferentially adherent compounds to compete for surface occupancy. Indeed, using an *in vitro* model system, prior addition of surfactant was demonstrated to significantly reduce thrombin production in gas-embolized whole blood and to attenuate platelet–platelet and platelet–bubble binding in similarly exposed plasma.[4,5]

Our laboratory has extensively explored computational models to simulate flow dynamics for an embolic model system, which incorporates transport and hydrodynamic properties associated with surfactant-based intervention.[6–10] Findings from this work predict surfactant promotion of bubble detachment from the vessel wall through modification of its adhesion characteristics.[11] These results were confirmed *in vivo* with direct observation of accelerated embolism bubble clearance from the microcirculation of the rat cremaster muscle after administration of exogenous surfactant.[12] The bubble-vessel adhesion force per unit surface was determined more precisely in Suzuki and Eckmann[13] using an *ex vivo* technique developed in part for this purpose, demonstrating again that surfactants greatly reduce the per unit area adhesion force. These studies also indicate that the adhesive force between the gas-embolism and endothelium is modulated by endothelial damage or heparinase digestion of the glycocalyx – a carbohydrate rich, membrane tethered network of proteoglycans and glycoproteins covering the endothelial luminal surface.

Herein, we bring our investigations from the macroscale to focus on micro/nano scale phenomena associated with the biomechanics of endothelial cell surface layer interaction with the air interface of the bubble. Novel techniques developed in this laboratory allow production and precise manipulation of microbubbles in live-cell fluorescence microscopy studies. A bubble is formed in the cell plate solution by pushing air with a micro-injector through a glass capillary pulled and ground so that its bevel opposes the buoyant force of the emerged bubble. The pipette and associated bubble are then moved on a three-stage micromanipulator into contact with human umbilical vein endothelial cells (HUVEC) loaded with the calcium-sensitive dye, Fluo-4, while imaging with the phase-contrast and fluorescent modes of an inverted microscope (Fig. 1). Thus, using time lapse imaging studies, modulation of intracellular calcium (Ca^{2+}) levels is monitored as a bubble is brought into contact with the endothelial cell surface.

We suspect that aberrant Ca^{2+} signaling plays a major role in the etiology of gas-embolic induced endothelial dysfunction. Ca^{2+} is a vital second messenger in virtually all endothelial cellular processes, and in particular, a transient rise in intracellular Ca^{2+} concentration $[Ca^{2+}]_i$ has been observed ubiquitously with mechanical perturbation of the EC. Such spurious Ca^{2+} signaling induced in the EC by mechanical and physiochemical forces imposed by a bubble could have serious consequences on the finely tuned signal transduction pathways of the cell. Recently published work from our laboratory showed that the lethality of direct bubble expulsion impact on bovine aortic endothelial cells (BAECs) is highly dependent on Ca^{2+} entry, providing an important stepping off point for this work.[14] Now we continue with an examination of HUVEC response to pathophysiologically relevant and controlled non-lethal bubble contact. Significantly, this work allows us to identify generative molecular mechanisms for bubble-induced Ca^{2+} signaling events in a human cell line. Thus defined, we may then address, through surfactant intervention, elimination of the first causes of endothelial bubble injury.

Live-cell single cell imaging of microbubble contact with a cell is geometrically analogous to early investigations of mechanically activated membranes in which a fire polished glass micropipette was used to prod endothelial cells. The mechanical perturbation induces an intracellular calcium influx shown in later work to be dependent upon an intact actin cytoskeleton and phospholipase.[15,16] Many apparently similar mechanical forces are imposed onto the cell by gentle deformation by a rounded pipette tip or by a bubble. The glass surface of the pipette tip, however, does not mimic the gas/liquid interfacial surface of the bubble, precluding studies into relevant surface interactions. The cell perturbation system described briefly above and further in Methods, is unique in providing us with an *in vitro* pathophysiological model with which to identify mechanosensitive components of the ESL, especially the glycocalyx, that are triggered by bubble contact. We may then trace the induced biomolecular pathways by which these mechanical signals are translated into a cellular response.

The complex structure of the glycocalyx works on many levels allowing it to function as a vasoprotective and regulatory entity that also senses and translates forces felt by the endothelium, ultimately determining individual cell morphology and function.[17–19] A productive strategy towards understanding how specific glycocalyx components contribute in the mechanotransduction of shear stress has been to selectively degrade glycosoaminoglycans (GAGs) from the endothelial surface and reassessing function. From one set of the studies, the heparan sulfate proteoglycans (HSPGs), syndecan and glypican have been implicated as mechanosensors of shear stress induced production of nitric oxide (NO).[20] Another research group showed HSPGs necessary for reorganization of intracellular structural components (*e.g.* F-actin, vinculin) upon flow adaptation.[18,20] Digestion of hyaluronan (HA) from the endothelial glycocalyx also interferes in the detection and amplification of flow-induced shear forces.[21,22]

These shear-stress experiments examine cellular responses to forces administered over hours to days; intravascular bubble interactions with the ESL are acute. Thus, to model gas-embolism *in vitro* more accurately, the experiments described in the current paper query glycocalyx involvement in mechanotransductional signaling initiated from bubble contact occurring over seconds, measuring cellular responses in the second to minute time frame. Transient intracellular Ca^{2+} increase observed upon bubble contact is characterized in the context of a similar transient response, induced by solid mechanical stimulation. Further, the surface-active perfluorocarbon (PFC), Oxycyte, is shown to inhibit bubble induced calcium response, while showing no effect on a glass bead induced signal. Finally, we examine the effects of specific enzymatic digestion of heparan sulfate (HS) and HA in order to better understand their role in the mechotransduction of bubble imposed forces and the physiochemical (mis)cues taken from gas/liquid interfacial interactions. Our results indicate mechanisms, which we discuss, by which the biomechanical signals from bubble contact are transduced to initiate a calcium transient. In particular, we propose that bubble contact mechanically perturbs a HSPG, probably one of the syndecans, which in turn initiates Ca^{2+} influx through activation of a stretch activated channel (SAC).

Materials and methods

Cell culture

Primary HUVEC cells were purchased from Life Line Cell Technologies (Walkersville, MD) and cultured in Corning tissue culture flasks with VascuLife® VEGF Cell Culture Complete Medium in humidified 5% CO_2 incubators until 80% confluence. Cells were split with 0.05% Trypsin/0.02% EDTA solution and either replated or suspended in cryopreservation solution (KryoLife, Lifeline) and stored in liquid nitrogen.

Cell preparation

At least 24 h and not more than 5 days before the day of experiment cells (LifeLine < passage five) were sparsely plated (3–5 K cells cm^{-2}) onto either 35 mm or 50 mm Mattek glass bottomed Petri dishes coated with either 0.5% gelatin or 2 μg cm^{-2} fibronectin. HBSS (no phenol-red, no bicarbonate, Invitrogen) was supplemented with 1% FBS (Sigma), 2 mM GlutaMax (Invitrogen), and 0.01% Heparin Sodium (Fisher Scientific) and brought to pH 7.4 for use as the measurement solution.

Dye loading

Cells were loaded with 1 μM Fluo-4, a cell-permeable, calcium sensitive dye for 10 min at room temperature, washed in DPBS, put in measurement solution and incubated at room temperature for 20 min to allow for complete de-esterification of the dye. Ethidium-Bromide dimer (500 nM, final concentration) was added before all experiments to monitor for membrane integrity loss or cell death.

Microscopy

All experiments were performed on an inverted Olympus IX70 microscope outfitted with a Chroma Photofluor metal halide light source (89 North, Burlington VT) and imaged with a Cooke SensiCamQE camera (PCO Imaging, Kelheim, Germany). IPLab software integrated with a Ludl focus position encoder and shutter-filter controller was used for data acquisition. Image time courses were obtained with an IPLab script: typically one frame per second for 300 s with each frame shuttered between the visible and fluorescence light source. The fluorescence shutter used two different excitation filter settings resulting in three parallel time courses for each experiment: phase contrast, green and red.

Pipette preparation

Bubbles were produced (described in detail below) with glass micropipettes prepared from 3.5″ Drummond glass capillaries (I.D. 0.53 mm, O.D. 1.14 mm) pulled in a Sutter Instruments, Model P-97 Flaming/Brown micropipette puller. The pulled pipette was then ground on a Narishige's EG-44 micropipette grinder at a 32.5° angle. The ground pipette was back loaded with measurement solution and sealed onto a microinjector (Nanoject, Drummond Scientific, Broomall, PA).

Microbubble experiment

Cell plates were placed on the stage of the microscope, which allows tracking and submicron movement of vertical position. The microinjector, with pipette tip fabricated as described above, was mounted on a three-stage micromanipulator (Piezo-Patch, World Precision Instruments Sarasota, FL). The mount was manually rotated to bring the glass tip into the center of the plate; piezo-electric motors on the stage were used for all further manipulation. Real time preview in the IPLab acquisition software (with the z-stage add-on) allowed visual positioning of cells, the pipette tip and the bubble. Lifting the tip above the surface of the liquid, air was pulled into the pipette with the microinjector, and the tip then positioned in the measurement solution of the plate 700–800 μm from the bottom. Slowly expelling the injector plunger pushed air out to form bubbles between 50–250 μm in diameter. The bubble was brought into position 100 μm over the cell of interest. At this point an IPLab script was initiated to capture images. The bubble was lowered gradually in 5 μm steps until it was observed to contact the cell surface in phase contrast imaging.

If necessary, the bubble was moved about the perinuclear region until a rapid and strong increase in Fluo-4 fluorescence intensity was observed. A schematic of the set up is shown in Fig. 1.

Glass bead experiments

Before use, 100 μm glass beads (Spectrum Laboratory Products, New Brunswick, NJ) were autoclaved, soaked in 10% Bovine Serum Albumin (BSA) then washed in sterile measurement solution. Cells were plated and dye loaded as described above. The plate was placed on the microscope stage, the cells to be probed were brought into focus and the image sequence collection IPLab script was started. The beads were released and dropped under gravity onto the plate at low density. With cell contact a calcium transient response was initiated.

Enzyme and inhibitor treatments

All enzymes and inhibitor compounds were purchased from Sigma Aldrich, St. Louis MO, except where noted. Treatment with cytochalasin D was performed in growth media at 100 nM for 1 h prior to dye loading. Heparinase I and Hyaluronidase were dissolved using manufacturer's recommendations. Cells in serum-free media (HBSS, glutamate and 1% BSA) were exposed to hyaluronidase (15 U/mL) for 1 h and heparinase I for 2 h at 37 °C. The heparinase treatment conditions have been previously reported to remove ~45% of the surface HS chains.[20] After treatment, cells were washed 3 times with DPBS, then dye-loaded as normal. Gadolinium (Gd^{3+}) and Ruthenium Red (RR) stock solutions were directly diluted to 10 μM and 1 μM, respectively, in the measurement plate before experiment. TRPV4 message in our HUVEC cell line was confirmed with reverse-transcriptase polymererization chain reaction (RT-PCR). TRPV4 channel function and activity of the selective TRPV4 antagonist, HC067047 (TOCRIS Bioscience, Ellsville, MO) was demonstrated with 4α-Phorbol 12,13-Didecanoate (4α-PDD). See Electronic Supplementary Information (ESI) for further details of Methods and Results for the RT-PCR and 4αPDD experiments. In the bubble experiments, HC067047 was dissolved at 10 mM DMSO and diluted to a final concentration of 1.5 μM into the measurement solution. Pre-treatment with 0.5 μM of phorbol 12-myristate 13-acetate (PMA) for 30 min at 37 °C in serum free media was used to induce syndecan ectodomain shedding. Syndecan-4 shedding was confirmed with immunofluorescence also detailed in ESI. Cells were also pretreated with PMA in the presence of 20 U/mL tissue inhibitor of metalloproteinase (TIMP-3, Sigma Aldrich, St. Louis MO) to inhibit syndecan ectodomain shedding with PMA induced PKC activation.[23] Glypican was depleted from the cell surface by pretreatment of cells with 1U/mL phosphotidyl inositol specific phospholipase C (PIPLC) in serum free medium for one hour before bubble probing experiments.[24] ATP (Fisher Scientific) was dissolved to 100 mM and brought to pH 7 in phosphate buffer and aliquoted for direct dilution into cell plate for control experiments. ATP provoked Ca^{2+} response of the cell plate was tested after each experiment in which inhibition of bubble induced transient response was observed, assuring that any given pretreatment did not detrimentally effect basic intracellular Ca^{2+} signaling machinery.

Surfactants

BSA (Sigma Aldrich) was dissolved to 10% (w/v) in measurement solution then sterile filtered and diluted directly into the cell plates before measurement. Oxycyte, a third-generation perfluorocarbon (PFC) therapeutic oxygen carrier (Oxygen Biotherapeutics) was diluted to 30% in measurement solution, sonicated briefly and syringe filtered (0.45 μM) to remove any large aggregates. The suspension was further diluted directly in the cell plates and allowed to sit for at least 5 min before measurement.

Additional exposures

Cells were sparsely plated and grown to ~10% confluence so that single and multi-cell configurations were present on each plate tested. In each experiment, bubble contact was made with an individual cell. However, for the various plate conditions, cell-cell contact effects were examined by choosing both cells having no adjacent neighbors and cells growing in small confluent groups from 2–20 cells. Multiple touch experiments were also performed by bringing the bubble in contact with the cell in a cellular location that elicits a response, while the IPLab acquisition script was running. The z-step function on the micromanipulator stage was then immediately toggled to step the pipette with attached bubble away from the cell in 5 μm increments. After a given time, depending on the particular experiment, the toggle was again reversed and the bubble stepped down in 5 μm increments until cell contact was remade in the same location. This procedure was then repeated iteratively.

Data analysis

Fluorescence intensity time courses from the microscopy images acquired were measured for each time point and then exported to Excel for further calculations. Normalized fluorescence traces were calculated for both the nuclear region of interest (ROI) and the cytoplasm ROI as:

$$\mathbf{F}_N(t) = (\mathbf{F}(t) - \mathbf{F}_b(t))/(\mathbf{F}_o - \mathbf{F}_b(t)) \quad (1)$$

where $\mathbf{F}(t)$ and $\mathbf{F}_b(t)$ are the average pixel intensities of the nuclear (or cytoplasmic) and background ROIs at each time point, respectively, and $\mathbf{F}_o$ is a stable baseline starting fluorescence for the particular region of interest. Time courses were shifted so that bubble contact is defined as $t = 0$. The maximum normalized fluorescence value after bubble contact is the parameter used for further statistical analysis with means and standard error measurements (SEMs) presented as bar chart values and error bars, respectively, in the figures. Reported p-values are results from unpaired Students t-tests calculated using the program GraphPad Prism version 5.00 for Windows (GraphPad Software, San Diego, CA). GraphPad Prism was also used for curve fitting analysis.

Results

Fig. 2 displays selected frames from a time dependent Ca^{2+} response image sequence reported by Fluo-4 for a HUVEC cell in our standard measurement medium during a typical bubble contact experiment. Time relative to bubble contact is indicated with line segments to appropriate data points on the

resultant nuclear ROI normalized transient time course, graphed as a solid line. Also shown in Fig. 2 are exemplar time courses for cells under conditions, noted in figure legend, in which the bubble induced calcium transient was inhibited: (1) pretreatment with 100 nM cytochalasin-D (2) with 10 μM Gd^{3+} (3) with 1 μM RR, (4) in low $[Ca^{2+}]_{EC}$, and (5) with 10% Oxycyte. In control bubble experiments the maximum in signal intensity occurred on average 23 s after initial contact. Bubble size varied from 60–250 μm in diameter with no dependence in the amplitude of $[Ca^{2+}]_i$ signal on bubble size. In our standard measurement medium, control cells displayed similar calcium transients after bubble contact in >97% of the cases. For comparison, a typical $[Ca^{2+}]_i$ signal after mechanical perturbation with a 100 μm glass bead is shown as a dotted gray line in Fig. 2. The solid glass-bead induced $[Ca^{2+}]_i$ transient occurred in every instance.

Fig. 3 shows a representative example of EC response to successive bubble touch events. The cell continues to respond to bubble contact, with decreasing Ca^{2+} signal peak intensities for nine consecutive contact events. Beyond this, cells do not recover from a non-responsive state. Though still viable by morphological and membrane integrity measures, an EC cell can no longer mobilize intracellular Ca^{2+} after up to 45 min resting time. Decreasing peak amplitude tracks with the number of contact events, not time between events. That is, the ratios of peak intensities from subsequent bubble touches are the same if touches occur from 20 to 360 s apart. The ratio of signal amplitudes (normalized to the maximum fluorescence amplitude F_N/F_{max}) with respect to event number is graphed as an inset in Fig. 3. The successive cell response is best fit to a one-site competition curve with variable slope.

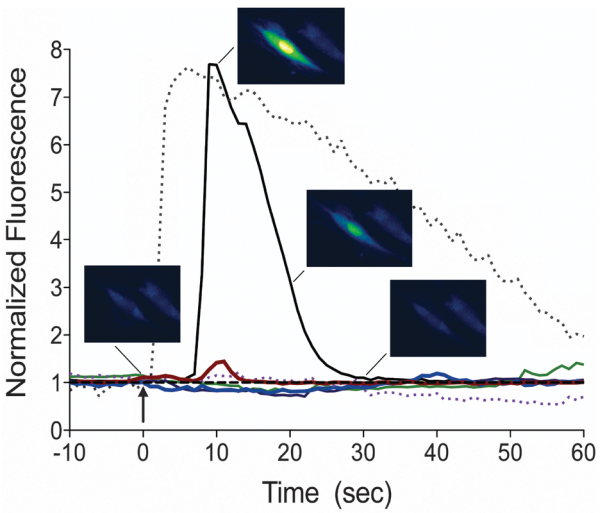

Fig. 2 Normalized Fluo-4 fluorescence time courses with contact occurrence indicated at $t = 0$ for (solid black line) control HUVEC contacted with a bubble and (dotted gray trace) HUVEC contacted with glass bead. Representative false-colored Fluo-4 intensity map images acquired and used to calculate the control bubble touch trace are shown with line segments to indicate occurrence during time course. Additional bubble contact $F_N(t)$ traces for HUVECs in conditions which inhibited response: (green) pretreated with 100 nM cytochalasin D; (purple) in 10 μM Gd^{3+}; (blue) in low external Ca^{2+}; (red) with 1 μM RR; and (dotted purple) in 10% Oxycyte.

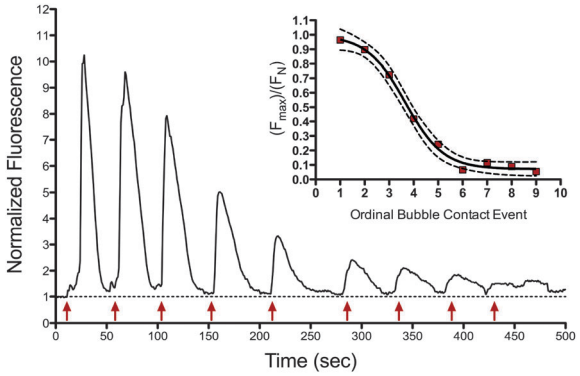

Fig. 3 $[Ca^{2+}]_i$ response of one cell to successive bubble contacts. Each bubble touch event is indicated with an arrow. Inset shows fractional maximum amplitude (F_N/F_{max}) as a function of bubble contact event number and the best fit to a one site competition curve with variable slope.

The mean amplitude dependence of the signal on extracellular calcium concentration, $[Ca^{2+}]_{EC}$, is shown with the bar chart of Fig. 4. Our standard measurement medium has $[Ca^{2+}]_{EC} = 2$ mM. Increasing $[Ca^{2+}]_{EC}$ to 20 mM shows a statistically significant ($p = 0.0286$) increase in the transient amplitude. When all Ca^{2+} in the HBSS measurement solution is replaced with Mg^{2+} (approximately 2 μM $[Ca^{2+}]_{EC}$ remains from FBS in cell medium), there is near elimination of any $[Ca^{2+}]_i$ increase from baseline upon bubble contact. Depolarization of the membrane potential with 150 mM KCl in the external medium did not result in a statistically significant change of the bubble-induced calcium transient (*data not shown*).

Pretreatment of the cells with cytochalasin D completely abolished any increase of internal calcium concentration upon bubble contact. Addition of Gd^{3+} or RR, an inhibitor of the TRPV superfamily of Ca^{2+} channel also eliminated any $[Ca^{2+}]_i$ increase normally induced by bubble contact. A selective and potent TRPV4 antagonist, HC067047, had no effect on cell responsiveness at 1.5 μM, five times the IC_{50}. Gd^{3+} did not inhibit calcium mobilization when cells were probed with the glass bead control.

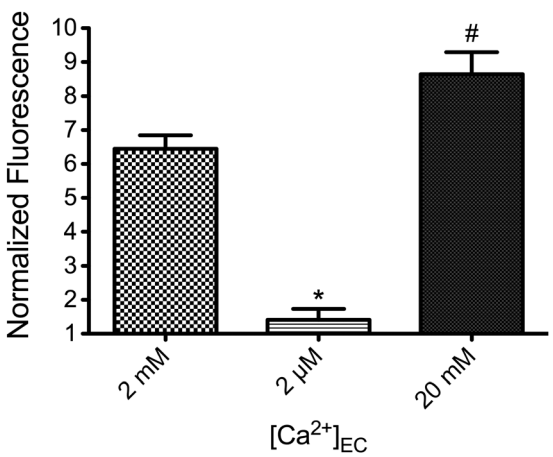

Fig. 4 Bar chart showing $F_N(t)$ amplitudes for control (2 mM), low (~2 μM) and high (20 mM) extracellular Ca^{2+} concentrations. (*) $p = 0.0001$; (#) $p = 0.0286$.

Fig. 5 illustrates surfactant effects on both bubble and bead induced intracellular calcium mobilization. Addition of 2.5% BSA reduced the percentage of transient occurrence upon bubble contact from almost 98% to 60%. The mean amplitude of the signal in the presence of BSA was not significantly reduced. Strikingly, addition of the PFC, Oxycyte (structure shown as inset), completely abolishes the calcium transient response of the cell in almost 78% of the cases. In the incidents in which cells did respond, the mean normalized calcium signal was 2.2 verses 6.2 times baseline for that of the control cells. When the Oxycyte is rinsed from the cell plates, the cells regain their full response to bubble contact (*data not shown*).

Still in Fig. 5, the transient Ca^{2+} signaling response of control cells to contact by 100 μm glass beads is shown to be slightly larger in amplitude than the response elicited by bubble contact (7.5 *vs.* 6.2), occurring more quickly after contact (2–5 s *vs.* ~20 s), and taking longer to return to a baseline, (> 60 s *vs.* ~20 s). Oxycyte has no inhibitory effect on cell response to bead perturbation. In fact, the average amplitude of $[Ca^{2+}]_i$ increase from bead contact is slightly but significantly higher than control with Oxycyte present.

Shown in Fig. 6 are example traces of a bubble induced calcium transient for control cells and cells after enzymatic treatment with heparinase I and hyaluronidase. A barchart indicating mean and S.E.M. values of the results from all these experiments is presented as an inset. Pretreatment with Heparinase I lowered the mean amplitude of Ca^{2+} mobilization. This enzymatic treatment had no inhibitory effect on glass bead-induced transients (*data not shown*). Treatment with hyaluronidase made engagement of the bubble with the cell very difficult. Bubbles, when brought in proximity were repulsed from the cell surface and displaced off the pipette. If bubble-cell contact could be made, the resulting Ca^{2+} upsurge was initiated on average more quickly after contact having essentially the same amplitude.

Fig. 7 illustrates the effect of selective HSPG depletion from the cell surface. The left panel graphs the mean normalized fluorescence amplitudes as occurred under conditions

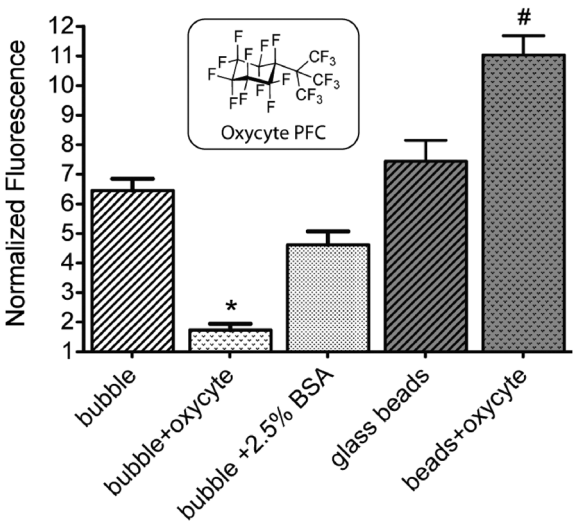

Fig. 5 Bar chart with BSA and Oxycyte effects on the mean bubble-induced amplitudes after bubble contact (*) $p < 0.0001$ (paired with bubble control) and Oxycyte effect on the mean glass-bead induced $F_N(t)$ amplitudes (#) $p = 0.017$ (paired with glass-bead control).

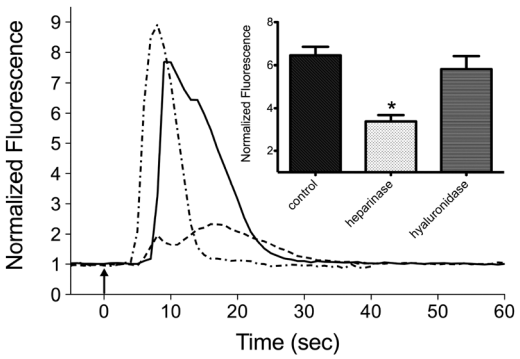

Fig. 6 Exemplar traces of Ca^{2+} response after bubble contact for HUVEC (solid) control; pretreated with (dash-dot) Hyaluronidase and (dashed) Heparinase I. (Inset) Bar chart with mean amplitudes of Ca^{2+} signaling for control and glycocalyx component digested samples (*) $p = 0.0004$.

specified: (1) control; (2) PMA; (3) PMA in the presence of TIMP-3; and (4) PIPLC. The right panel shows percentage of cells from the total probed that displayed bubble-induced Ca^{2+} transients. Control cells displayed Ca^{2+} transients after bubble contact in 98% of the incidences with average amplitudes of 6.2 over baseline fluorescence. Depletion of syndecan-1 and syndecan-4 ectodomains whose shedding was induced by PMA prior to the experiment reduced the mean normalized fluorescence amplitude of responding cells to 2.2 times baseline with only 8% of the cells responsive to bubble probing. Immunofluorescence staining experiments showed ~70% depletion of cell surface syndecan-4 (data shown in ESI).

When PMA pretreatment was performed in the presence of TIMP-3, an inhibitor of the metalloprotease responsible for syndecan cleavage, >40% of the cells responded with signal amplitudes statistically unchanged from control. When 1 μM (final concentration) ATP was added to the dual PMA/TIMP-3 treated cells, an intracellular upsurge of Ca^{2+} in response to the ATP occurred in only ~50% of cells, whereas cells treated only with PMA to which ATP was added demonstrated retention of full activity (data not shown). Finally, cleavage of GPI linked

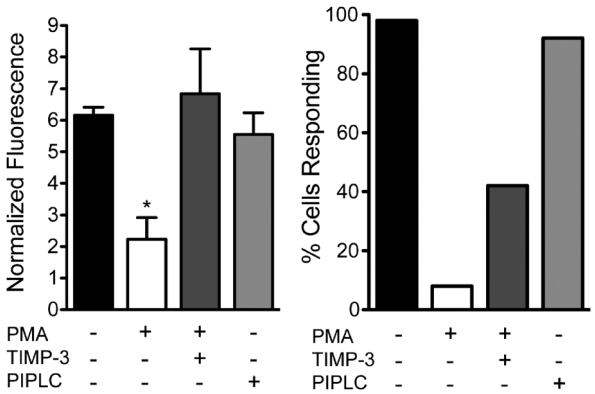

Fig. 7 Barcharts indicating effects of targeted HSPG depletion from the cell surface prior to bubble probe experiments. (Left panel) Mean bubble-induced transient amplitudes and ± SEM of responding cells after pretreatment as indicated below (*) $p = 0.0194$. (Right panel) percent of cells tested that responded to bubble touch in the same experiments.

glypican from the cell surface by pretreatment with PIPLC resulted in no significant change from control in the responsiveness of cells or mean amplitude of bubble induced Ca^{2+} transients.

Cell-cell contact effects were tested by perturbing both single cells and cells growing in nearly confluent groups of two to twenty. There was no statistical change in the amplitude or morphology of Ca^{2+} transients from single cell experiment if the targeted cell was in the presence other cell. Also, cells adjoining the one that was subjected to bubble contact did not display any Ca^{2+} transients (*i.e.* bubble contact does not induce signaling extracellularly). An example of this lack of communication between adjoining cells is seen in the time frame images of Fig. 2. There are two cells in the field of view. One cell is hit by a bubble and responds accordingly with an intracellular Ca^{2+} transient. The cell to the right, not contacted with a bubble, remains at resting $[Ca^{2+}]_i$ throughout. Propagation of a Ca^{2+} signal from the contacted cell to neighboring and further removed cells was observed with glass bed perturbation.

Discussion

The multifaceted chemical structure of the glycocalyx allows the underlying endothelium to function as an interpretive and regulatory interface between circulating blood and the rest of the vasculature. Our cell perturbation system provides a powerful tool with which to unravel the complex interactions between gas/liquid interfacial forces and components of the glycocalyx, for *in vitro* exploration of relevant pathophysiology in vascular air embolism. Thus, we may carefully investigate currently unexplored mechanisms that have been suggested by previous work from our laboratory using a similar technique. In this previous work the lethality of direct bubble expulsion over BAECs was linked to the magnitude of Ca^{2+} and NO response after bubble impact. Additionally, the authors demonstrated that use of the surfactants, Pluronic F-127 and/or albumin, attenuated the lethality of microbubble contact to this cell line.[14]

With real time live-cell imaging through controlled non-lethal microbubble contact, we show that bubble contact with a HUVEC results in a strong mobilization of intracellular Ca^{2+}. Upon repeated or extended bubble adherence to the ESL, we hypothesize that continued induction of intracellular Ca^{2+} transients leads to aberrant cell function through initiation of biochemical pathways, which we now are just beginning to identify. In this present work, however, we focus on early mechanotransduction events of cellular response and identify a specific mechanism of action for surfactant intervention as the glycocalyx transfers direct mechanical and chemical cues from luminal gas/liquid interfacial interactions, through to transmembrane components, initiating Ca^{2+} influx.

There is significant reduction of occurrence in transient $[Ca^{2+}]_i$ increases if bubble contact is made in the presence of either surfactants tested, BSA and the PFC, Oxycyte. These results support our hypothesis that bubble surface adherence of ESL macromolecules initiates cellular response, and that surfactants will attenuate this response by direct competition for interfacial occupancy. Indeed, in this mode, Oxycyte proves an extremely efficient interfacial adsorbent that all but eliminates any bubble-induced Ca^{2+} response of the cell. Viewed in light of earlier computational, *ex* and *in vivo* studies from our laboratory, Oxycyte emerges as an exciting potential treatment for intravascular bubble injury. It prevents mechanotransductional insult by ameliorating development of adhesion forces between the bubble and the ESL. Further, Oxycyte inhibits activation of Ca^{2+} influx notwithstanding sustained bubble contact.

Previous investigations into the mechanotransduction machinery of endothelial cells have used several approaches to apply forces to cells. In the single cell studies of Diamond *et al.*,[15] endothelial cells (BAEC and HUVEC) were prodded with a fire polished glass micropipette resulting in a mechanically induced Ca^{2+} transient. In the current work, we reproduce these results using 100 μm glass beads to contact the cell. With findings from the two studies, we can now compare (and contrast) EC response to bubble contact with that of a similarly sized solid probe. The time courses of Ca^{2+} signaling after either method of perturbation are similar. In both cases, a touch results in a strong transient $[Ca^{2+}]_i$ increase, which returns to baseline within close to a minute. Besides similar fluorescence time courses, there are other characteristics shared between the differently provoked EC responses. Each induced transient requires an influx of Ca^{2+} from the extracellular milieu, and in both cases influx will not occur if cytoskeletal structure is compromised with cytochalasin D, an inhibitor of actin polymerization.

Differences in the underlying mechanisms behind the two Ca^{2+} signals are revealed when we investigate (1) how extracellular Ca^{2+} enters the cell and (2) what triggers this influx. Mechanically gated SAC mediated Ca^{2+} influx has been shown to be an important local initiating event especially in the endothelial control mechanisms of focal adhesion and shear stress response.[25] In fact, for the gas/liquid interface imposed forces of our system, the SAC inhibitor, Gd^{3+}, eliminated any Ca^{2+} transient upon bubble contact. Moreover, RR also inhibited intracellular Ca^{2+} mobilization while cell response to the bubble was unchanged in the presence of the potent and specific TRPV-4 antagonist HC067047, thus identifying the SAC to be a member of the TRPV superfamily but not TRPV-4. Neither Gd^{3+} nor RR had any effect, however, on bead-initiated responses. Likewise, while Oxycyte completely abolished any bubble-induced Ca^{2+} transient; it showed no inhibitory effect whatsoever upon Ca^{2+} transients after bead contact. Thus, solid mechanical and bubble induced Ca^{2+} transient events, while similar in morphology and amplitude, arise from different mechanical signaling mechanisms. The bead induced Ca^{2+} signal, impervious to both surfactant and channel inhibition, activates ion flux through channel(s), other than SACs, perhaps by simple compressive force on the ESL and associated glycocalyx, or by direct contact with mechanosensing elements in the cell membrane. The material properties of Oxycyte appear to slightly amplify transmission of this compressive force and/or effective surface area of the bead, thus modestly increasing the amplitude of the glass bead induced signal. This amplification may be the result of additional cell membrane or cell surface deformation induced by the added mass of Oxycyte plus glass beads, over that of the beads alone, settling onto the cell surface. In the case of bubble contact with the cell, the resulting Ca^{2+} transient is reliant on active TRPV channels. Activation of TRPV is inhibited by surfactant, which indicates glycocalyx

involvement in channel opening. Preferential interfacial occupancy by Oxycyte disallows the glycocalyx interactions necessary in the TRPV gating mechanism.

The more specific nature of triggering surface interactions and subsequent TRPV activation was investigated with a focus on two glycocalyx GAG components. HA and HS were targeted for selective depletion from the glycocalyx through enzymatic digestion prior to experiment. The left panel of Fig. 8 shows a simplified schematic of the EC components particularly relevant to this study. Implications of the observed changes in intracellular Ca^{2+} response following HA/HS enzymatic cleavage are discussed below. In particular, directed digestion of these GAG components indicate that the glycocalyx is instrumental in regulating bubble induced Ca^{2+} transient events through (1) protection by HA of the underlying cell membrane from deformation forces visibly imposed by the bubble and (2) TRPV activation *via* interfacial interaction with HS.

It is apparent from the phase contrast frames of the time course experiments that membrane deformation alone by the bubble is not sufficient to initiate a Ca^{2+} response. Visual verification of cell surface contact defines the $t = 0$ frame, and in our control experiments $[Ca^{2+}]_i$ levels do not start to rise until seconds after this first touch. This delay in the Ca^{2+} signaling after interfacial contact can be opposed to the immediate (within the 1 s time resolution of the experiment) response after contact by the glass bead. For a bubble, signal initiation is also dependent on the cell surface location of contact. A bubble held in continued engagement with a cell, which has no initial Ca^{2+} response, does not, in the time course of the experiment, ever trigger a response. Thus, the channel activation moiety does not appear to diffuse freely in the plasmalemma.

When the three-dimensional polysaccharide network formed by HA (represented by gray random coil lines in Fig. 8) is degraded through directed enzyme hydrolysis, activation by the bubble occurs on average more quickly after cell contact. Establishing this contact is also more difficult

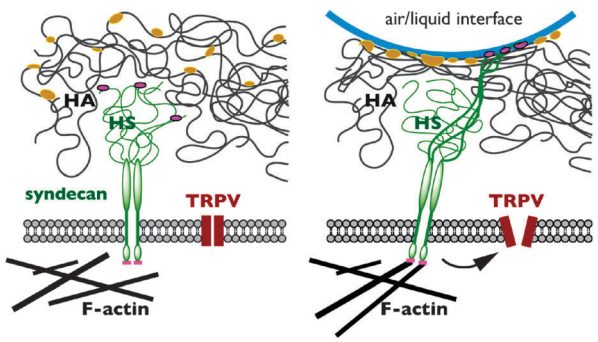

Fig. 8 Simplified schematic of glycocalyx and cell plasma membrane components in left panel, and proposed mechanism of bubble induced transient $[Ca^{2+}]_i$ increase in the right panel: HA is shown as grey lines with brown ovals representing associated plasma proteins. Syndecan HS side chains (green) are pulled into the bubble air/liquid interface (represented by a blue arc) when HS bound protein ligands (purple ovals) adhere to its surface. The resultant tensile force physically displaces a transmembrane syndecan (shown as dimer), altering cytoplasmic domain actin cytoskeleton associations (purple rectangles) and activating a TRPV Ca^{2+} channel.

after HA depletion – repulsive forces push the bubble away from the cell and around the restraining edge of the pipette. Once initiated, however, the resulting signal amplitude does not change from control. These results indicate that HA functions not as an activating entity but rather as a cushion or barrier between the active air/liquid interface and underlying components of the glycocalyx. Such mitigating role for HA concurs with theoretical models that have incorporated known glycocalyx component structural parameters. Linked to the plasma membrane only through non-covalent binding associations with HA synthase, chondroitin sulfate, and cell surface receptors such as CD44, the HA forms a porous and dynamic gel layer with a characteristic hydraulic permeability that is predicted to dissipate any fluid shear-stress so that the underlying plasma membrane is subjected to essentially zero force.[26]

In microscopic imaging experiments the HA component of the glycocalyx appears almost like that of cotton candy on the cell surface, extending microns from the luminal cell surface.[27] It is certainly is one of the first ESL macromolecular entities the bubble gas/liquid interface encounters as it approaches the cell. A recent fluorescence correlation spectroscopy study shows HA to be a major determinant in albumin recruitment in the assembly of plasma proteins that forms on the vessel wall surface.[28] Removal of these associated proteins upon HA digestion explains the loss of bubble adherence observed in our study as they would normally be drawn to the bubble surface. With some steric hindrance imposed by HA to the gas/liquid interface as it approaches the cell, the non-specifically bound protein component contributes interfacial competition that kinetically limits specific interactions necessary for TRPV activation.

HS, the second glycocalyx component targeted, makes up 50–90% of endothelial cell surface GAGs.[29] The HS component is represented in Fig. 8 as green traces attached to a HSPG, syndecan. Most HS exists as side chains of two major families of EC surface proteoglycans, the syndecans and the glypicans. The HSPG are instrumental in several aspects of shear-stress mechanotransduction, especially shear-induced NO production.[20] In our study we observe a significant reduction in bubble contact induced Ca^{2+} signaling in cells, which have had their surface HS population depleted through specific enzyme digestion.

Selective depletion of syndecan from the cell surface through PMA induced ectodomain shedding resulted in nearly complete loss of the Ca^{2+} transient response to bubble contact. We further show that the cellular calcium response to bubble contact was restored when the protease responsible for syndecan ectodomain shedding was inhibited by presence of TIMP-3 during PMA pretreatment. Additionally, we targeted the second major family of cell surface HSPGs, the glypicans, using PIPLC to cleave the GPI anchored proteoglycans from the outer leaflet of the cell membrane. PIPLC pretreatment elicits no significant change in either the occurrence frequency or amplitude of bubble induced Ca^{2+} transient response. These results, summarized in Fig. 7, indicate syndecan to be the HSPG essential for normal HUVEC response to air/liquid interfacial interaction.

One model of shear-stress mechanotransduction proposes that flow forces physically displace membrane-spanning proteoglycans, which in turn perturb cytoskeletal structures to which they are intracellularly linked.[30] Extrapolating from

shear stress mechanotransduction to transduction of forces developed during gas/liquid/glycocalyx interfacial interactions, a proposed mechanically based initiation molecule requires connections to both extra- and intracellular structures. The extracellular domain of a mechanotransducer also requires sensitivity to mechanical signals impinged by the bubble, and the intracellular domain must have associations with pertinent structural and signaling proteins. The extracellular domains of syndecan and glypican both fill the requirements to act as tensile force sensors. Their structurally complex extracellular polysaccharide side chains extend apically, and as multifunctional regulators of protein activities, HS protein binding motifs are specific and highly regulated.[31,32] HS interacts with a broad spectrum of extracellular protein ligands, and these bound proteins provide the mechanism for mechanical signaling. The proteins will partition to the bubble interface, and pull with them the attached HSPG.

Glypican does not have an intracellular domain, however. Its membrane attachment occurs through a covalent linkage to glycosylphosphatidylinositol (GPI), which localizes glypican to caveolae. These specialized membrane rafts are microdomains for many signal transduction functions, including the regulation of endothelial nitric oxide synthase activity.[33] More relevant to the Ca^{2+} signaling work of this current investigation are the syndecans expressed in endothelial cells, syndecan-1 and syndecan-4. They are type-I transmembrane proteins giving them connectivity between extracellular HS side chains, which can function as tensile force sensors, and their cytoplasmic domains capable of interacting with the actin cytoskeleton and interceding signal cascades.[34,35]

Syndecan-4, especially, has been the subject of particular interest as a novel transducer of mechanical stimuli. Most work has examined syndecan-4 in terms of its interaction with the ECM and its role in the assembly of focal adhesions and stress fibers.[36–39] On the apical cell surface, however, syndecans had long been considered "ligand gatherers", working as co-receptors with other signaling proteins.[40] While there is much evidence that syndecans on the cell surface may function to signal independently, investigations into such roles are challenged by difficulties in application of local forces to the apical cell surface. One recent work has revealed very rapid SAC activation in response to strain forces applied through manipulation of magnetic beads bound specifically to EC surface integrins.[41] As in our study, ion flux was not activated by deformation of the lipid bilayer alone. Channel activation required specific mechanical strain on the cytoskeletal backbone of the focal adhesions that form around the magnetic beads as they bind the cell surface. Thus the mechanical strain was provided by integrin as it was pulled with the magnetic bead.

Our current study suggests an analogous architecture on the apical cell surface. This architecture can be probed with the physiochemically active gas/liquid interface of the bubble. Our data strongly support a model, illustrated in the right panel of Fig. 8, for initiation of a bubble induced Ca^{2+} transient. The bubble imposes tensile force on a HSPG—our data indicate the transmembrane syndecan—as proteins ligands bound to the HS side chains are pulled into the hydrophobic gas/liquid interface. This force physically displaces syndecan, and its actin-associated cytoplasmic domain, to subsequently perturb cytoskeletal structure and activate a TRPV calcium channel. The specific gating mechanism for the TRPV remains unknown, but this event initiates ion influx and the bubble induced Ca^{2+} signal. We show the proposed triggering HS interfacial interactions, and therefore any resultant bubble-induced cell injury, may be prevented with surfactant Oxycyte. Oxycyte efficiently adheres to the gas/liquid interface, coating its surface with a biologically inert compound, to compete with any glycocalyx or plasma macromolecule interactions.

Acknowledgements

The authors gratefully acknowledge support for this work by ONR N00014-08-1-0436, ONR N00014-10-1-0074 and NIH R01 HL67986. Our sincere thanks to Bo Han and Dr. Max Kelz for their technical advice and use of equipment for RT-PCR; and to Ge Liang for technical assistance.

References

1 D. E. Graham and M. C. Phillips, *J. Colloid Interface Sci.*, 1979, **70**, 403–414.
2 D. E. Graham and M. C. Phillips, *J. Colloid Interface Sci.*, 1979, **70**, 415–426.
3 D. E. Graham and M. C. Phillips, *J. Colloid Interface Sci.*, 1979, **70**, 427–439.
4 D. M. Eckmann and S. L. Diamond, *Anesthesiology*, 2004, **100**, 77–8.
5 D. M. Eckmann, S. C. Armstead and F. Mardini, *Anesthesiology*, 2005, **103**, 1204–1210.
6 K. Mukundakrishnan, P. S. Ayyaswamy and D. M. Eckmann, *J. Biomech. Eng.*, 2009, **131**, 074516-1-5.
7 K. Mukundakrishnan, P. S. Ayyaswamy and D. M. Eckmann, *Phys. Rev. E: Stat., Nonlinear, Soft Matter Phys.*, 2008, **78**, 036303-1-15.
8 K. Mukundakrishnan, D. M. Eckmann and P. S. Ayyaswamy, *Ann. N. Y. Acad. Sci.*, 2009, **1161**, 256–267.
9 K. Mukundakrishnan, S. P. Quan, D. M. Eckmann and P. S. Ayyaswamy, *Phys. Rev. E: Stat., Nonlinear, Soft Matter Phys.*, 2007, **76**, 036308-1-17.
10 J. Zhang, D. M. Eckmann and P. S. Ayyaswamy, *J. Comput. Phys.*, 2006, **214**, 366–396.
11 T. N. Swaminathan, K. Mukundakrishnan, P. S. Ayyaswamy and D. M. Eckmann, *J. Fluid Mech.*, 2010, **642**, 509–539.
12 A. Suzuki, S. C. Armstead and D. M. Eckmann, *Anesthesiology*, 2004, **101**, 97–103.
13 A. Suzuki and D. M. Eckmann, *Anesthesiology*, 2003, **99**, 400–408.
14 S. Kobayashi, S. D. Crooks and D. M. Eckmann, *Undersea Hyperb. Med.*, 2011, **38**, 27–39.
15 S. L. Diamond, F. Sachs and W. J. Sigurdson, *Arterioscler., Thromb., Vasc. Biol.*, 1994, **14**, 2000–2006.
16 W. J. Sigurdson, F. Sachs and S. L. Diamond, *Am. J. Physiol. Heart Circ. Physiol.*, 1993, **264**, H1745–H1752.
17 A. R. Pries, T. W. Secomb and P. Gaehtgens, *Pfluegers Arch.*, 2000, **440**, 653–666.
18 M. M. Thi, J. M. Tarbell, S. Weinbaum and D. C. Spray, *Proc. Natl. Acad. Sci. U. S. A.*, 2004, **101**, 16483–16488.
19 J. M. Tarbell and M. Y. Pahakis, *J. Intern. Med.*, 2006, **259**, 339–350.
20 J. A. Florian, J. R. Kosky, K. Ainslie, Z. Pang, R. O. Dull and J. M. Tarbell, *Circ. Res.*, 2003, **93**, e136–e142.
21 S. Mochizuki, H. Vink, O. Hiramatsu, T. Kajita, F. Shigeto, J. A. E. Spaan and F. Kajiya, *Am. J. Physiol. Heart Circ. Physiol.*, 2003, **285**, H722–H726.
22 S. Mochizuki, H. Vink, O. Hiramatsu, H. Nakamoto, Y. Ogasawara, J. A. E. Spaan and F. Kajiya, *FASEB J.*, 2003, **17**, A1241–A1241.
23 M. L. Fitzgerald, Z. H. Wang, P. W. Park, G. Murphy and M. Bernfield, *J. Cell Biol.*, 2000, **148**, 811–824.
24 K. Ding, M. Lopez-Burks, J. A. Sanchez-Duran, M. Korc and A. D. Lander, *J. Cell Biol.*, 2005, **171**, 729–738.

25 C. K. Thodeti, B. Matthews, A. Ravi, A. Mammoto, K. Ghosh, A. L. Bracha and D. E. Ingber, *Circ. Res.*, 2009, **104**, 1123–1130.
26 S. Weinbaum, X. B. Zhang, Y. F. Han, H. Vink and S. C. Cowin, *Proc. Natl. Acad. Sci. U. S. A.*, 2003, **100**, 7988–7995.
27 K. Rilla, R. Tiihonen, A. Kultti, M. Tammi and R. Tammi, *J. Histochem. Cytochem.*, 2008, **56**, 901–910.
28 A. P. Stevens, V. Hlady and R. O. Dull, *Am. J. Physiol.: Lung Cell. Mol. Phys.*, 2007, **293**, L328–L335.
29 S. Reitsma, D. W. Slaaf, H. Vink, M. A. M. J. van Zandvoort and M. G. A. O. Egbrink, *Pfluegers Arch.*, 2007, **454**, 345–359.
30 P. F. Davies, *Physiol. Rev.*, 1995, **75**, 519–560.
31 M. Bernfield, M. Gotte, P. W. Park, O. Reizes, M. L. Fitzgerald, J. Lincecum and M. Zako, *Annu. Rev. Biochem.*, 1999, **68**, 729–777.
32 J. Turnbull, A. Powell and S. Guimond, *Trends Cell Biol.*, 2001, **11**, 75–82.
33 H. H. Patel and P. A. Insel, *Antioxid. Redox Signaling*, 2009, **11**, 1357–1372.
34 A. C. Rapraeger, *J. Cell Biol.*, 2000, **149**, 995–998.
35 A. Yoneda and J. R. Couchman, *Matrix Biol.*, 2003, **22**, 25–33.
36 S. Saoncella, F. Echtermeyer, F. Denhez, J. K. Nowlen, D. F. Mosher, S. D. Robinson, R. O. Hynes and P. F. Goetinck, *Proc. Natl. Acad. Sci. U. S. A.*, 1999, **96**, 2805–2810.
37 A. Woods and J. R. Couchman, *Curr. Opin. Cell Biol.*, 2001, **13**, 578–583.
38 F. Denhez, S. A. Wilcox-Adelman, P. C. Baciu, S. Saoncella, S. Lee, B. French, W. Neveu and P. F. Goetinck, *J. Biol. Chem.*, 2002, **277**, 12270–12274.
39 R. M. Bellin, J. D. Kubicek, M. J. Frigault, A. J. Kamien, R. L. Steward, H. M. Barnes, M. B. DiGiacomo, L. J. Duncan, C. K. Edgerly and E. M. Morse, *et al.*, *Proc. Natl. Acad. Sci. U. S. A.*, 2009, **106**, 22102–22107.
40 J. R. Couchman, *Nat. Rev. Mol. Cell Biol.*, 2003, **4**, 926–937.
41 B. D. Matthews, C. K. Thodeti, J. D. Tytell, A. Mammoto, D. R. Overby and D. E. Ingber, *Integr. Biol.*, 2010, **2**, 435–442.

